Supporting Information

1 Experimental Section

1.1 Materials and synthesis

General information: PM6 and D18 were purchased from Solarmer Materials Inc. L8-BO，Y6 and BTP-eC9 were purchased from eFlex PV. The detailed synthetic routes of SD62 were depicted below. The synthesis of SD62 required the synthesis of Compound 1,2 and 3 in advance, shown as **Scheme S1**. Compound 1 and Compound 2 were synthesized according to literatures.[1, 2] Other reagents were purchased from Energy Chemical (Sun Chemical Technology (Shanghai) Co., Ltd.) or Bide Pharmatech Ltd. Unless otherwise stated, analytical grade solvents and commercially available reagents were used without further purification. Chromatography columns were packed with 200-300 mesh silica gel in petroleum ether (bp. 60-90 ºC). The chemical shifts (δ) were given in part per million relatives to internal tetramethyl silane (TMS, 0 ppm for ^{1}H) and $CDCl_3$ (77.0 ppm for ^{13}C). All chemical shifts (δ) were reported in ppm and coupling constants (*J*) in Hz.

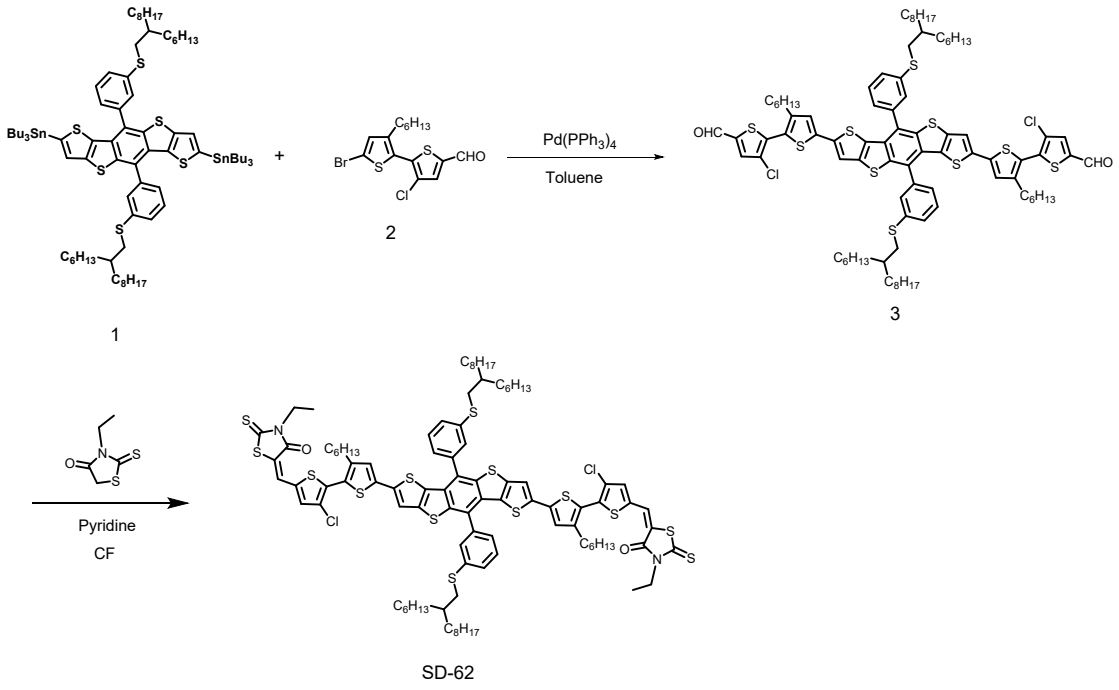

Scheme S1. Synthetic route of SD-62.

Synthesis of compound 3: Compound 1 (309 mg, 0.200 mmol), Compound 2 (86 mg, 0.220 mmol), and $Pd(PPh_3)_4$ (23 mg, 0.020 mmol) were dissolved in deoxygenated toluene. The reaction mixture was refluxed for 24 h and then extracted with dichloromethane (DCM). The collected organic layer was dried over anhydrous $MgSO_4$. After removal of the solvent under reduced pressure, the residue was purified by silica gel chromatography (petroleum ether (PE)/chloroform (CF), v/v = 1:1) as eluent and then recrystallized from methyl alcohol to give a red product (152 mg, 48%). ^{1}H NMR (600 MHz, $CDCl_3$, δ/ppm) δ 9.84 (s, 2H), 7.65 (s, 2H), 7.61-7.56 (m, 6H), 7.43 (d, J = 7.2 Hz, 2H), 7.31 (s, 2H), 7.01 (s, 2H), 2.99 (d, J = 9.0 Hz, 4H), 2.61 (t, J = 7.8 Hz, 4H), 1.74-1.70 (m, 2H), 1.62-1.58 (m, 4H), 1.46-1.35 (m, 8H), 1.32-1.20 (m, 52H), 0.88-0.82 (m, 18H). ^{13}C NMR (151 MHz, $CDCl_3$, δ/ppm) δ 181.75, 145.36, 141.42, 140.97, 139.93, 139.82, 139.51, 138.97, 138.46, 137.79, 136.38, 132.79, 129.86, 129.56, 128.85, 128.81, 126.23, 126.21, 125.44, 124.41, 116.83, 77.25, 77.04, 76.83, 38.33, 38.31, 37.61, 33.26, 33.22, 33.21, 31.92, 31.85, 31.82, 31.56, 30.48, 29.98, 29.94, 29.63, 29.60, 29.57, 29.37, 29.34, 29.12, 26.62, 26.60, 26.58, 26.55, 26.53, 22.70, 22.67, 22.60, 14.14, 14.09 (Note: some peaks in ^{13}C NMR spectrum

overlap).

Synthesis of SD62: Under nitrogen atmosphere, a mixture solution of Compound 3 (120 mg, 0.076 mmol), 3-ethyl-2-thioxothiazolidin-4-one (61 mg, 0.377 mmol), piperidine (0.5 mL), and CF (25 mL) was added to a 50 mL round bottom flask and then refluxed for 24 h. After cooling to room temperature, the mixture was poured into methanol and then filtered. The residue was purified by column chromatography on silica gel using a mixture solvent as eluent (PE/CF, v/v = 1:2) to give a black purple solid (106 mg, 75%). ^{1}H NMR (600 MHz, $CDCl_3$, δ/ppm) δ 7.72 (s, 2H), 7.61-7.57 (m, 6H), 7.46-7.45 (d, J = 6.6 Hz, 2H), 7.32 (s, 2H), 7.29 (s, 2H), 7.01 (s, 2H), 4.21-4.17 (m, 4H), 2.99 (d, J = 9.6 Hz, 4H), 2.63 (t, J = 8.1 Hz, 4H), 1.74-1.70 (m, 2H), 1.64-1.58 (m, 4H), 1.47-1.35 (m, 8H), 1.30-1.20 (m, 58H), 0.89-0.83 (m, 18H). ^{13}C NMR (151 MHz, $CDCl_3$, δ/ppm) δ 191.34, 167.10, 145.04, 141.33, 139.97, 139.75, 139.40, 138.73, 137.73, 136.40, 135.50, 133.58, 132.67, 129.78, 129.52, 129.47, 128.76, 126.26, 126.19, 126.14, 124.49, 123.13, 122.77, 116.66, 39.98, 38.26, 37.53, 33.14, 31.84, 31.77, 31.74, 31.52, 30.48, 29.86, 29.63, 29.56, 29.52, 29.49, 29.26, 29.12, 26.49, 26.47, 26.45, 22.62, 22.57, 14.07, 14.04, 12.20 (Note: some peaks in ^{13}C NMR spectrum overlap). MS (MALDI-TOF) m/z Calcd. For $C_{98}H_{118}Cl_2N_2O_2S_{14}$: 1874.4653, Found 1874.4356.

1.2 Device Fabrication and Testing

The solar cell devices were fabricated with a structure of Glass/ITO/PEDOT:PSS (20nm, purchased from Xi'an Polymer Light Technology Corp 4083)/Active layer/PNDIT-F3N/Ag. Pre-patterned ITO coated glass substrates (purchased from South China Science & Technology Company Limited, the sheet resistance of the ITO glass was about 10) were washed with methylbenzene, deionized water, acetone, and isopropyl alcohol in an ultrasonic bath for 15 minutes each. After blow-drying by high-purity nitrogen, all ITO substrates were cleaned in the ultraviolet ozone cleaning system for 15 minutes. Subsequently, a thin layer of PEDOT: PSS was deposited through spin-coating at 4,000 rpm for the 30s on the pre-cleaned ITO-coated glass from a PEDOT:

PSS aqueous solution and annealed at 150 ℃ for 15 min in atmospheric air. Then the photovoltaic layers were spin-coated in a glovebox. To obtain devices with different thickness (around 100 nm, 200 nm, 300 nm and 400 nm), the active layers, including the binary blends (PM6:L8-BO, PM6:Y6, PM6:BTP-eC9 and D18:L8-BO) and the ternary blends (PM6:SD62:L8-BO, PM6:SD62:Y6, PM6:SD62:BTP-eC9 and D18:SD62:L8-BO), were spin-coated from different concentrations (16 mg mL^{-1}, 24 mg mL^{-1}, 36 mg mL^{-1} and 48 mg mL^{-1}) dissolved in chloroform. The donor/acceptor (D:A) weight ratios were 1:1.2 (binary) and 0.8:0.2:1.2 (ternary) and the mixed materials were dissolved in chloroform solution with 0.3% additive of 1,8-diiodooctane (DIO) by volume, then stirred at 40 ℃ for 2 hours. The mixed solutions were spin-coated at 3500 rpm for 30 s, then an extra pre-annealing at 100 ℃ for 5 minutes was performed. Then methanol solution of PNDIT-F3N (0.5 mg mL^{-1}) was spin-coated onto the active layer at 4000 rpm for 30 s in a nitrogen atmosphere. Finally, the top argentum electrode of 100 nm thickness was thermally evaporated through a mask onto the cathode buffer layer under a vacuum of $\sim 5\times10^{-6}$ mbar. The typical active area of the investigated devices was 5 mm^2. The current-voltage (*J-V*) characteristics of the solar cells were measured by a Keithley 2400 source meter unit under AM1.5G (100 mW cm^{-2}) irradiation from a solar simulator (Enlitech model SS-F5-3A). Solar simulator illumination intensity was determined at 100 mW cm^{-2} using a monocrystalline silicon reference cell with KG5 filter.

The large-area modules were fabricated with the same architecture as small area solar cells. The ITO-coated glass substrates (5 cm × 5 cm) were patterned with 532 nm nanosecond laser beam and cleaned with detergent, deionized water and isopropanol. The PEDOT:PSS solution (100 μL) was deposited through blade-coating at 10 mm/s on pre-cleaned ITO-coated glass from a PEDOT: PSS: IPA=1:3 aqueous solution and annealed at 140 °C for 5 mins in atmospheric air. Next, the active layer materials in CF with a concentration of 16 mg mL^{-1} (100 μL) was blade-coated onto the PEDOT:PSS with a coating velocity of 15 mm s^{-1} and a gap height of 50 μm in the air. For green processing using toluene as solvent, the active layer materials were resolved with a

concentration of 18 mg mL^{-1}. Then the active layers were annealed at 100 °C for 7 min in glove box. The substrate temperature is about 40 °C when blade coating. And then the organic layers were partially removed by solvent-assisted mechanical scribing (thread wiping) for subsequent serial interconnection of the individual solar cells. Then methanol solution of PNDIT-F3N at a concentration of 1.0 mg mL^{-1} was blade-coated onto the active layer at 2 mm/s. When coating, the ambient temperature is about 25 °C and the ambient humidity is about 20%. To complete the fabrication of the devices, 100 nm of Ag was thermally evaporated through a mask under a vacuum of ~ 5×10^{-6} mbar, during which each single solar cell was monolithically interconnected. The current-voltage characteristics of the solar cells were measured under AM 1.5G irradiation on an Enli Solar simulator (100 mW cm^{-2}). Before each test, the solar simulator was calibrated with a standard single-crystal Si solar cell (made by Enli Technology Co., Ltd., Taiwan, calibrated by The National Institute of Metrology (NIM) of China).

1.3 Instruments and measurements

Absorption spectra: Ultraviolet-visible (UV-vis) absorption was measured using a PerkinElmer Lambda 1050 Spectrometer.

Electrochemical measurements: All cyclic voltammetry (CV) curves were measured by films cast from $CHCl_3$ solution on the glassy carbon electrode with Pt wire as the counter electrode and Ag/AgCl as reference electrode.

Thickness measurement: The thicknesses of active layers were measured by a Bruker Dektak XT stylus profilometer.

Grazing incidence wide-angle X-ray scattering (GIWAXS) measurements: GIWAXS measurements were performed at beamline 7.3.3 at the Advanced Light Source (ALS). Samples were prepared on Si substrates using identical blend solutions as those used in devices. The 10 KeV X-ray beam was incident at a critical grazing angle of 0.14°, which maximized the scattering intensity from the samples. The scattered X-rays were

detected using a Dectris Pilatus 1-M photon counting detector. Samples were prepared on Si substrates. All measurements were conducted under helium atmosphere to reduce air scattering.

Atomic force microscopy (AFM) measurements: AFM measurements were performed with a Nano Wizard 4 atomic force microscopy (JPK Inc. Germany) in Qi mode to observe the surface morphologies of the blend films deposited on glass substrates.

Photoluminescence (PL) measurements: The PL data and emission of relevant films were collected using a Zolix Flex One Spectrometer. The PL excitation wavelength was set to 532 nm and 639 nm.

Space Charge Limited Current (SCLC) Measurements: Electron and Hole mobility were measured using the space charge limited current (SCLC) method, the ITO substrates were ultra-sonicated in the same way for solar cell and the architecture: Glass/ITO/ZnO/Active layer/PNDIT-F3N/Ag for electron mobility (Glass/ITO/PEDOT: PSS/Active layer/MoO_x/Ag for hole mobility) measurement was prepared. The mobility was obtained by taking current–voltage curves and fitting the results to a space charge limited form.

Transient photocurrent (TPC) measurements: Relevant solar cells were excited with a 405 nm laser diode. The transient photocurrent response of the devices at short circuit condition to a 200 μs square pulse from the LED with no background illumination. The current traces were recorded on a Tektronix DPO3034 digital oscilloscope by measuring the voltage drop over a 5-ohm sensor resistor in series with the solar cell. DC voltage was applied to the solar cell with an MRF544 bipolar junction transistor in common collector amplifier configuration.

Transient Photovoltage (TPV) Measurements: In the TPV measurements, a 405 nm laser diode was used to keep the organic solar cells in the V_{OC} conditions. Measuring the light intensity with a highly linear photodiode and driving the laser intensity with a waveform generator (Agilent 33500B) allowed reproducible adjustments of the light

intensities over a range from 0.1 to 2.1 suns. Moreover, a small perturbation was induced with a second 405 nm laser diode. The intensity of the short laser pulse was adjusted to keep the voltage perturbation below 10 mV. After the pulse, the voltage decayed back to its steady-state value in a single exponential decay.

2. Experimental data

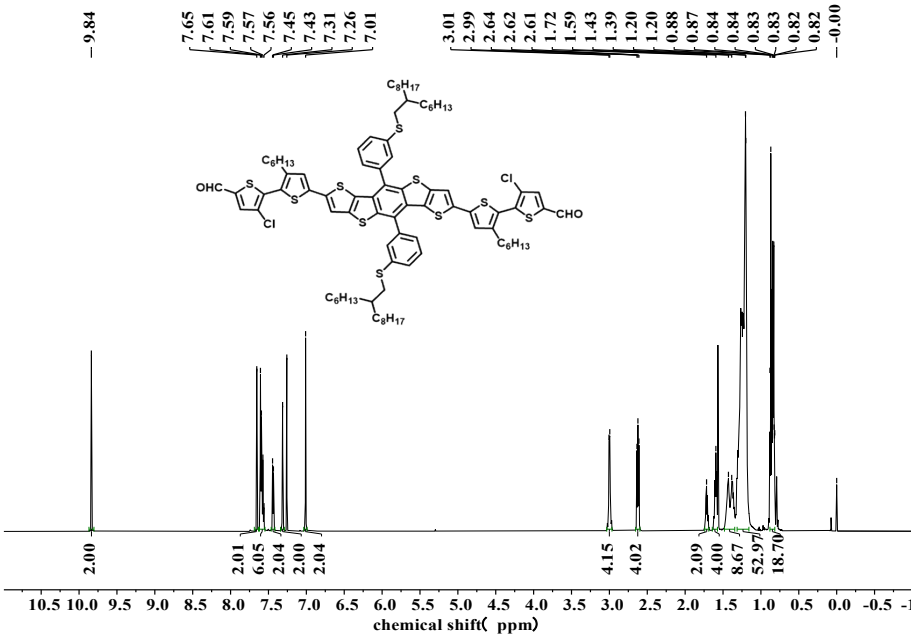

Figure S1. ^{1}H NMR spectrum of compound 3.

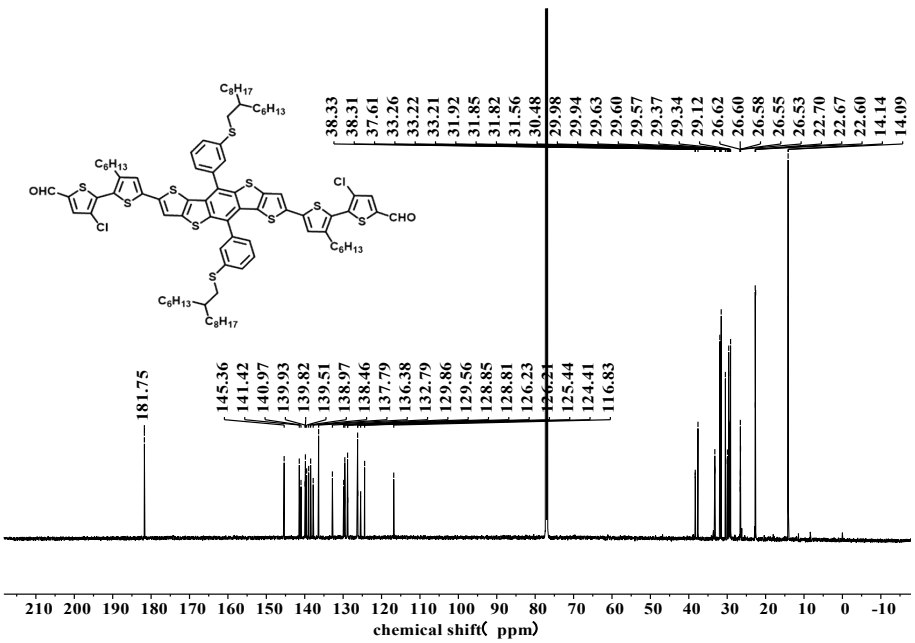

Figure S2. ^{13}C NMR spectrum of compound 3.

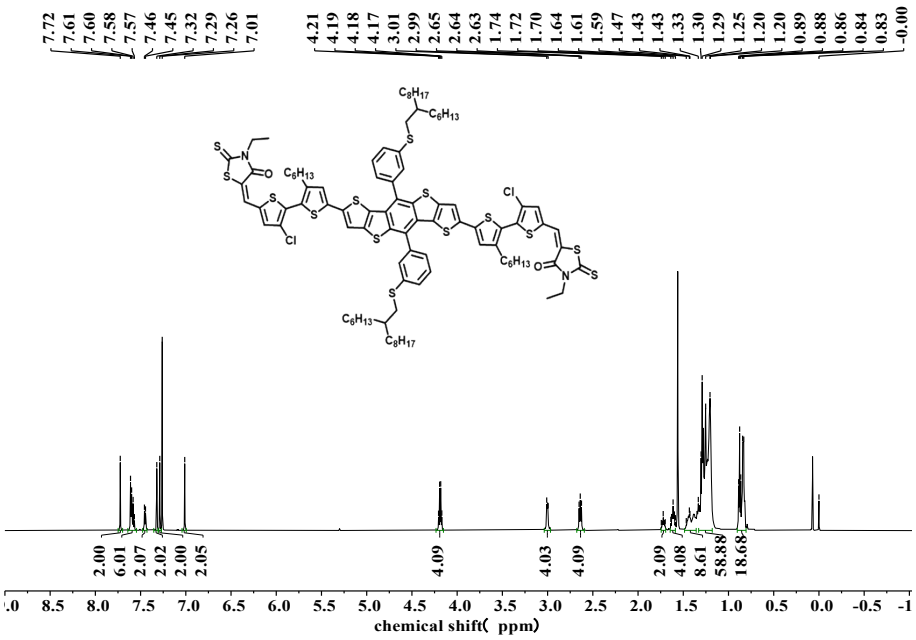

Figure S3. ^{1}H NMR spectrum of SD62.

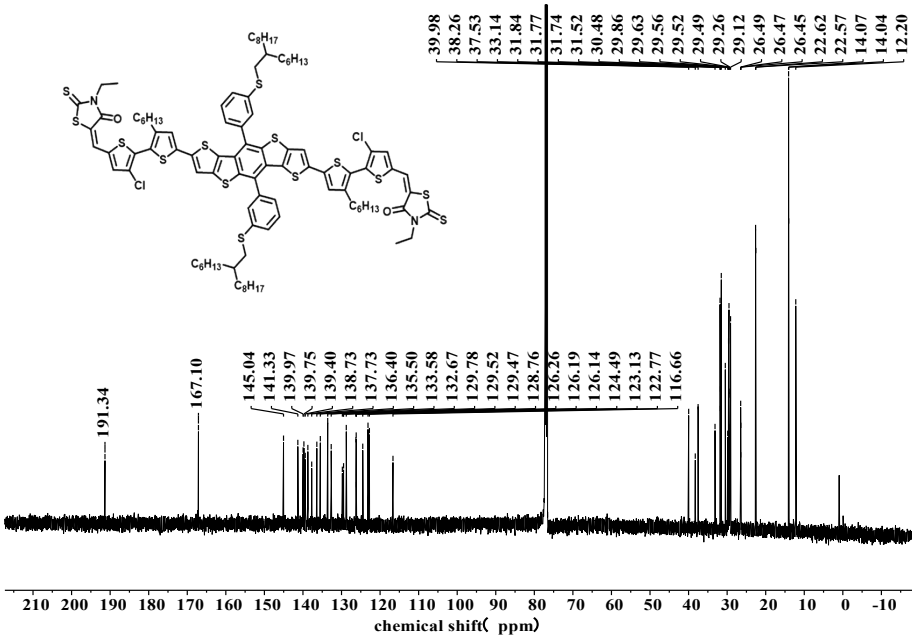

Figure S4. ^{13}C NMR spectrum of SD62.

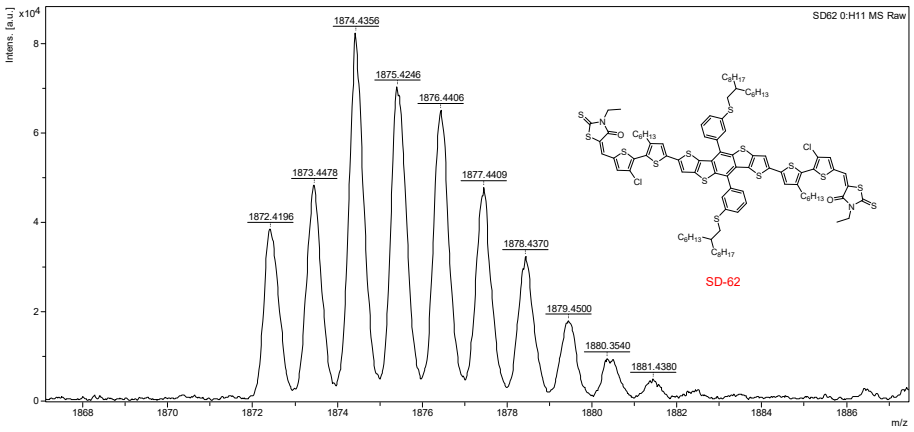

Figure S5. MALDI-TOF spectrum of SD62.

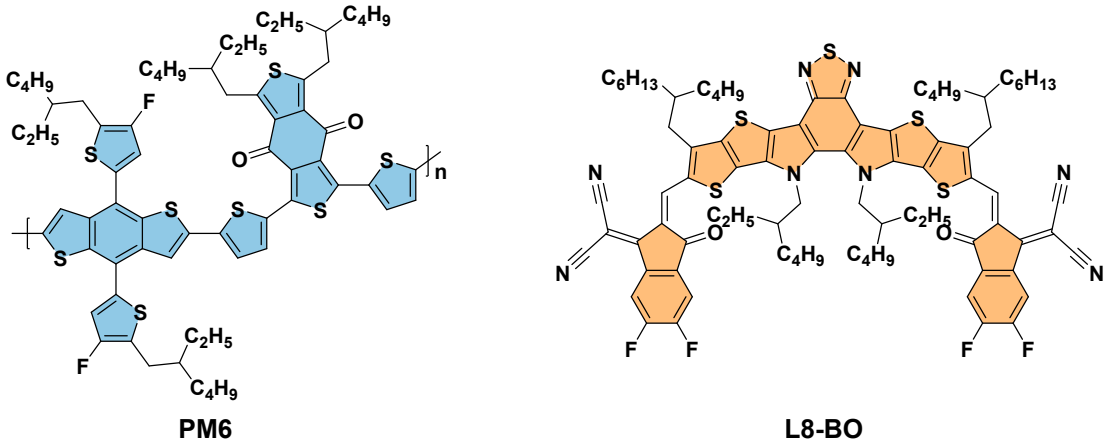

Figure S6. Chemical structures of the investigated PM6 and L8-BO materials.

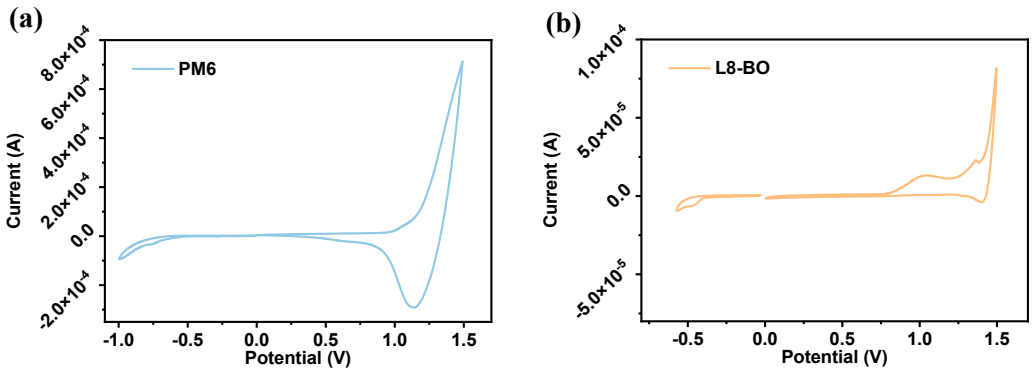

Figure S7. The CV curves of (a) PM6 and (b) L8-BO on Pt electrode in 0.1M Bu4NPF6, CH3CN solution.

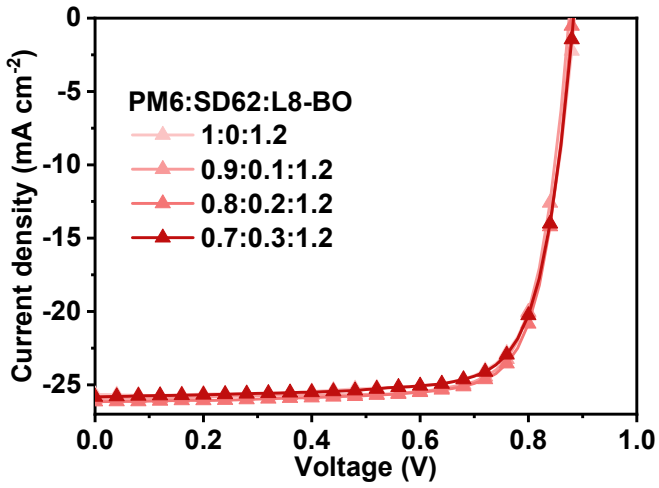

Figure S8. *J-V* curves of the ernary organic solar cells with different SD62 contents measured under the illumination of AM 1.5G at 100 mW cm^{-2}.

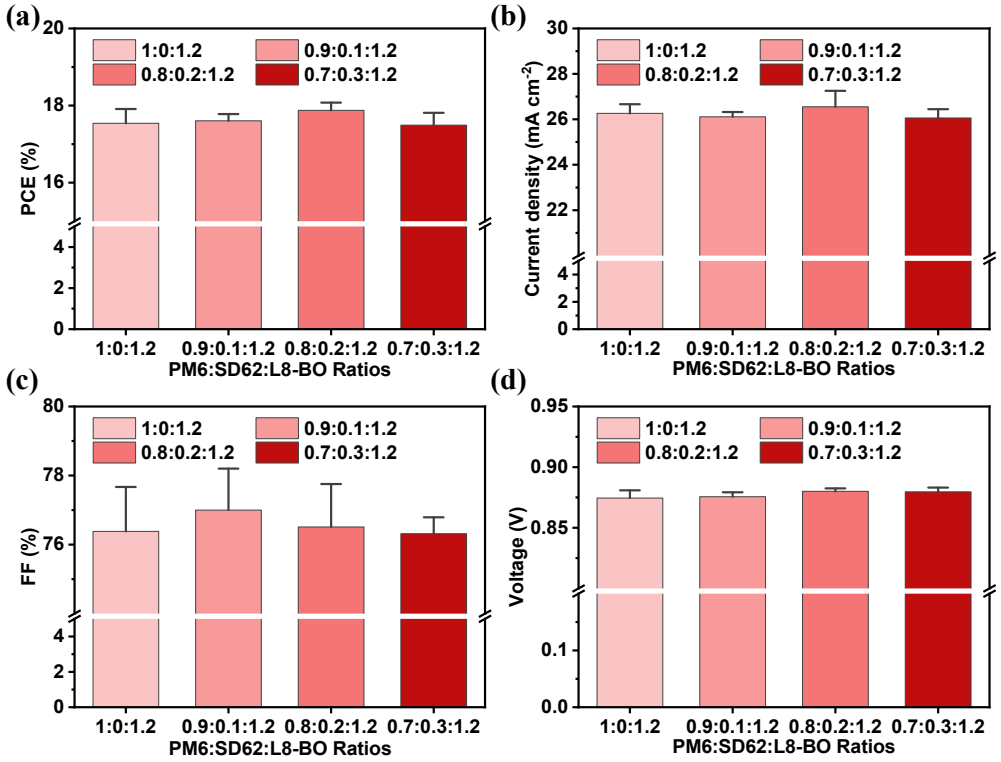

Figure S9. Photovoltaic parameters distribution of devices with different SD62 contents for (a) PCE; (b) J_{SC}; (c) FF; (d) V_{OC}.

Table S1. Photovoltaic parameters of the ternary solar cells with different SD62 contents, measured under the illumination of AM 1.5G at 100 mW cm^{-2}.

PM6:SD62:L8-BO	Thickness [nm]	V_{OC} [V]	J_{SC} [mA cm^{-2}]	FF [%]	PCE [%]
1:0:1.2	100	0.871 (0.875±0.004)	25.82 (26.26±0.38)	77.67 (76.38±1.30)	17.47 (17.54±0.25)
0.9:0.1:1.2	100	0.875 (0.876±0.002)	25.94 (26.11±0.14)	78.20 (77.00±0.95)	17.75 (17.60±0.21)
0.8:0.2:1.2	100	0.882 (0.880±0.002)	26.08 (26.55±0.45)	77.75 (76.51±0.88)	17.88 (17.87±0.14)
0.7:0.3:1.2	100	0.883 (0.880±0.002)	25.82 (26.06±0.28)	76.72 (76.32±0.62)	17.49 (17.49±0.24)

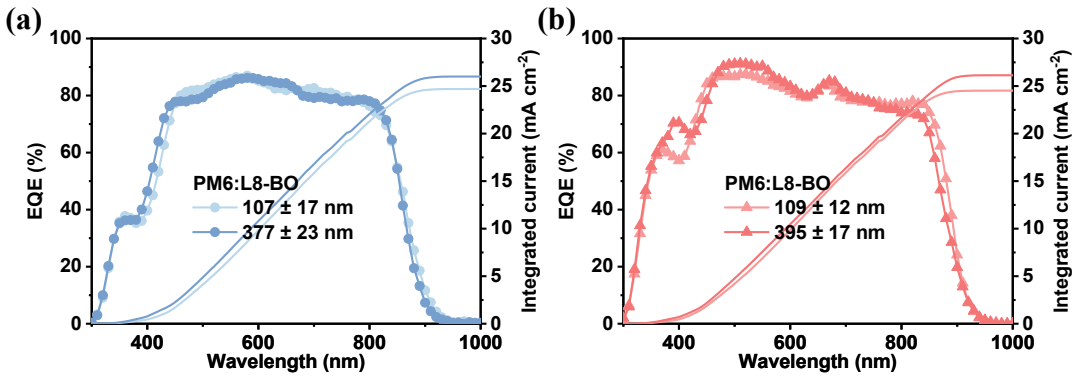

Figure S10. External quantum efficiency (EQE) curves of the (a) PM6:L8-BO binary with active layer thicknesses of 107±17 nm and 377±23 nm and (b) PM6:SD62:L8-BO ternary devices with active layer thicknesses of 109±12 nm and 395±17 nm, respectively.

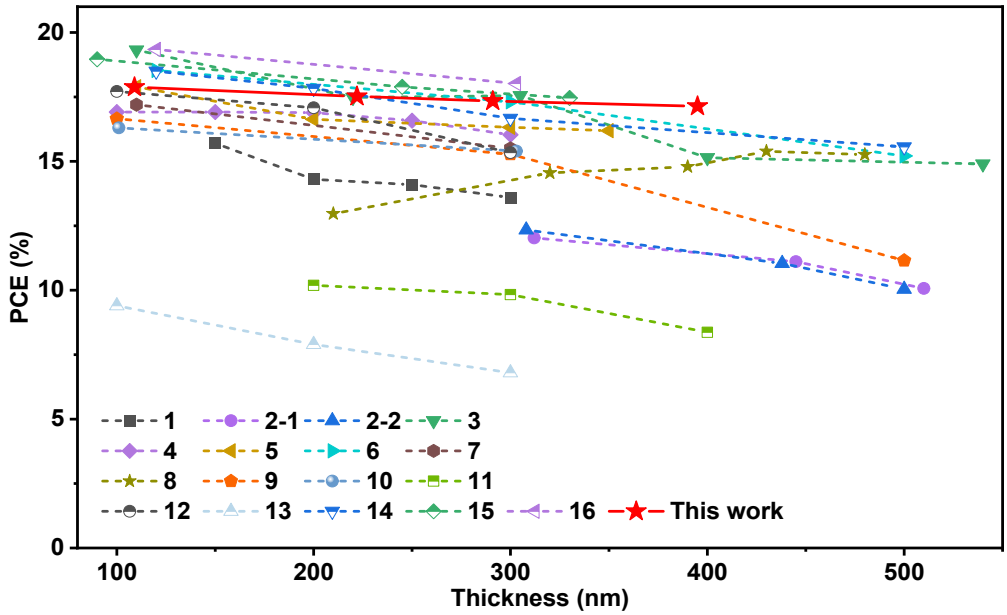

Figure S11. The dependence of PCE on film thickness in the organic photovoltaic systems.

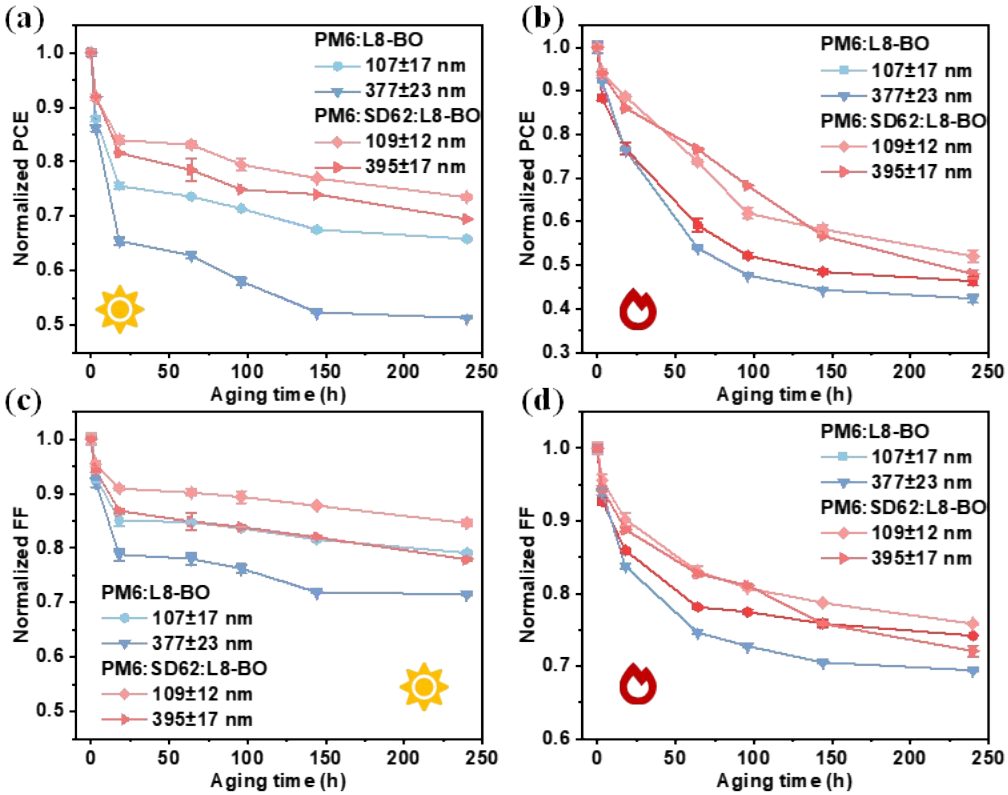

Figure S12. The normalized PCE degradation trends of relevant devices under (a) light soaking and (b) elevated temperature; The normalized FF degradation trends of relevant devices under (c) light soaking and (d) elevated temperature.

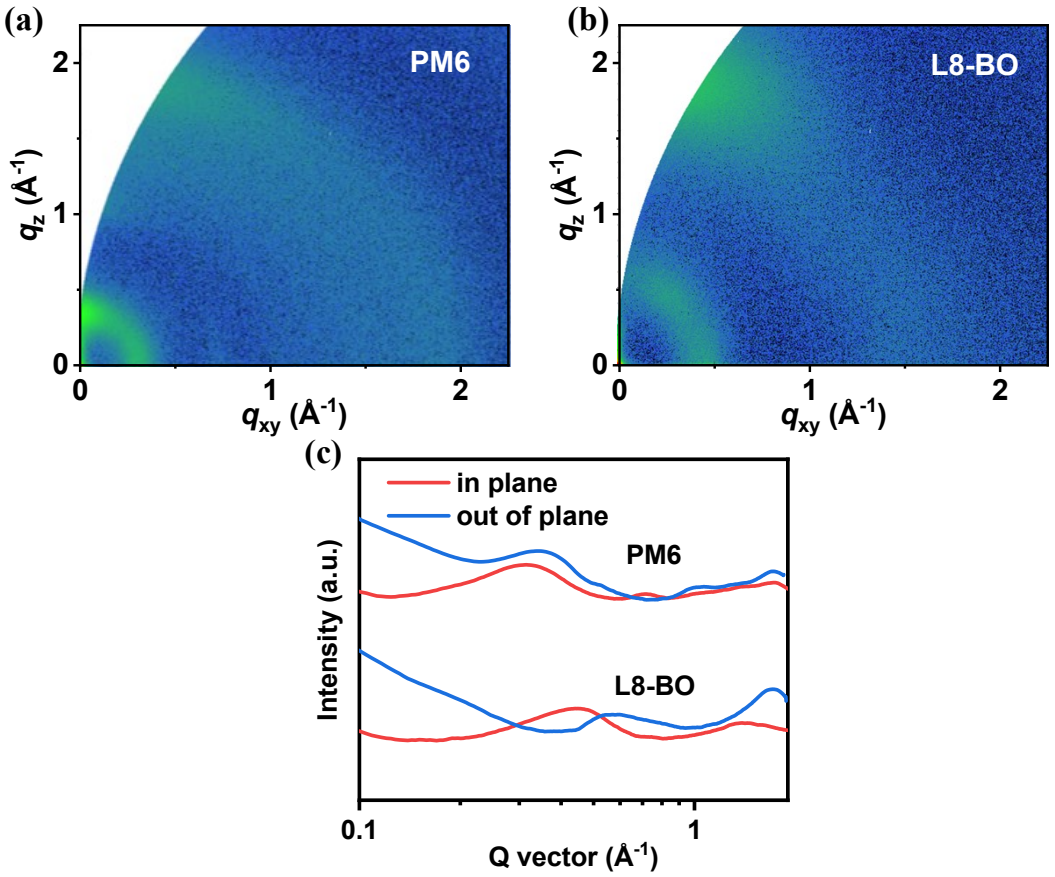

Figure S13. 2D GIWAXS patterns of pristine (a) PM6 and (b) L8-BO; (c) IP and OOP extracted line-cut profiles of relevant films.

Table S2. Investigations of the morphology parameters extracted from the GIWAXS measurements of the PM6, SD62 and L8-BO neat films.

Materials	In plane (q_x)				Out of plane (q_z)			
	Lamellar stacking (100)				π-π stacking (010)			
	q (Å^{-1})	d (Å)	FWHM (Å^{-1})	CCL (Å)	q (Å^{-1})	d (Å)	FWHM (Å^{-1})	CCL (Å)
PM6	0.314	19.982	0.126	49.711	1.722	3.647	0.208	30.200
SD62	0.321	19.585	0.100	62.675	1.699	3.696	0.757	8.293
L8-BO	0.439	14.299	0.183	34.356	1.711	3.670	0.677	9.275

Table S3. Investigations of the morphology parameters extracted from the GIWAXS measurements of the binary and ternary blend films with different blend thicknesses.

Materials	In plane (q_x)				Out of plane (q_z)			
	Lamellar stacking (100)				π-π stacking (010)			
	q ($Å^{-1}$)	d (Å)	FWHM ($Å^{-1}$)	CCL (Å)	q ($Å^{-1}$)	d (Å)	FWHM ($Å^{-1}$)	CCL (Å)
PM6:L8-BO (107±17 nm)	0.347	18.088	0.113	55.570	1.756	3.577	0.529	11.874
PM6:L8-BO (377±23 nm)	0.345	18.181	0.120	52.351	1.752	3.584	0.523	11.997
PM6:SD62:L8-BO (109±12 nm)	0.344	18.239	0.106	59.296	1.742	3.605	0.364	17.257
PM6:SD62:L8-BO (395±17 nm)	0.347	18.123	0.104	60.182	1.754	3.579	0.310	20.290

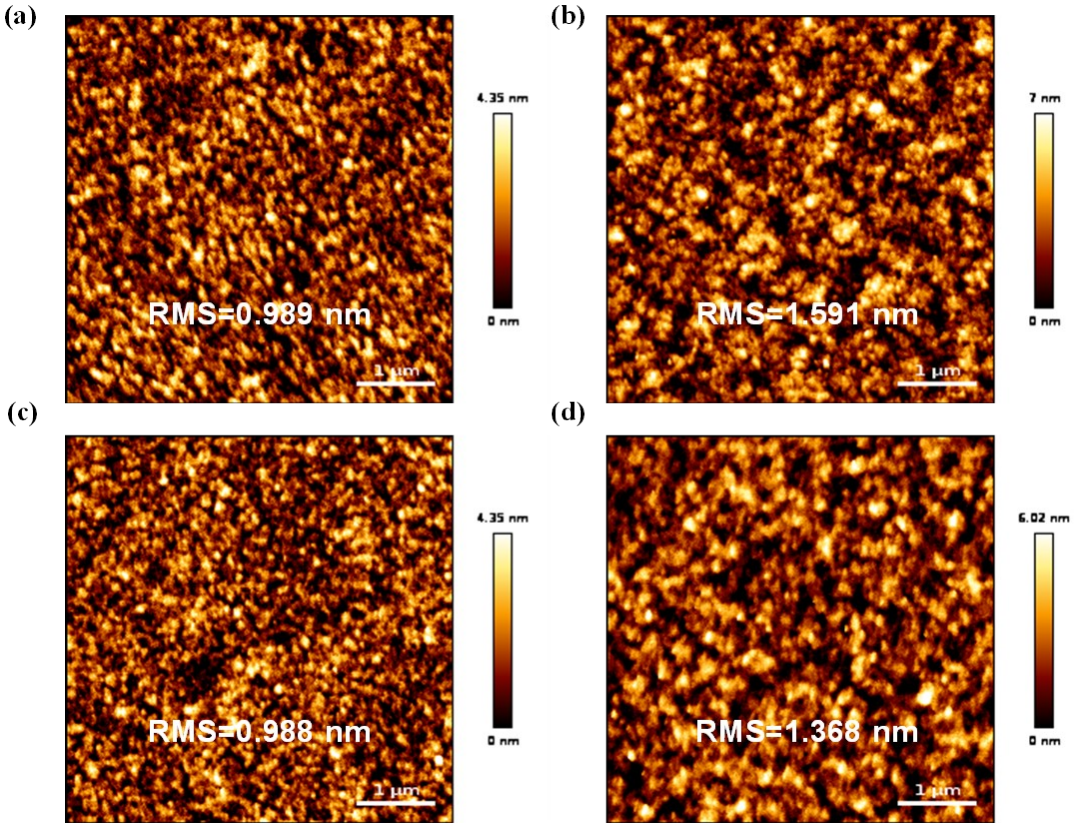

Figure S14. AFM height images of (a) PM6:L8-BO (107±17 nm), (b) PM6:L8-BO (377±23 nm), (c) PM6:SD62:L8-BO (109±12 nm) and (d) PM6:SD62:L8-BO (395±17 nm), respectively.

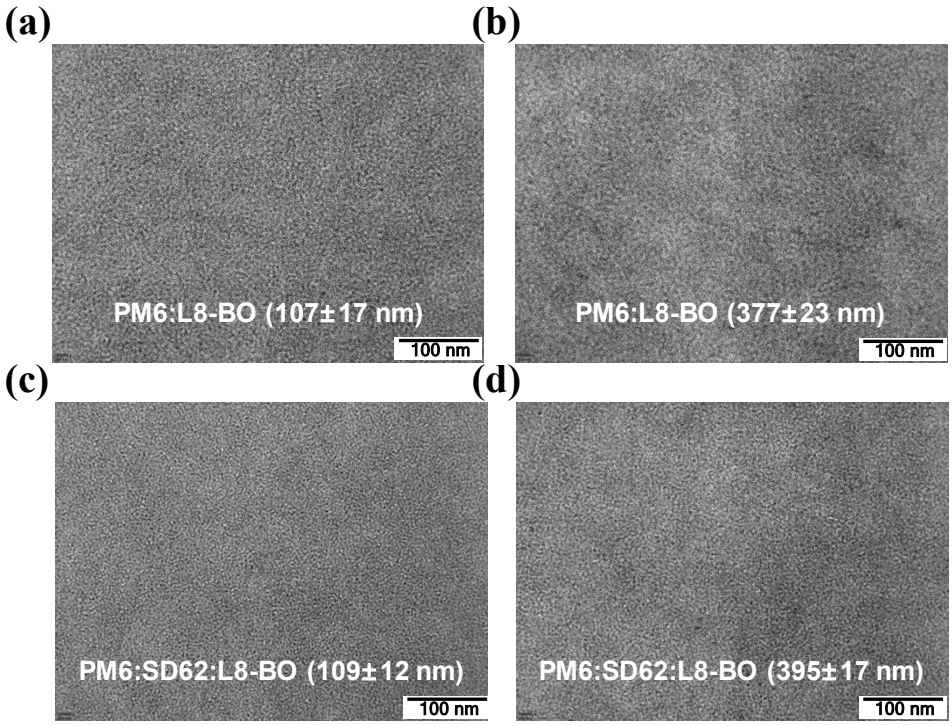

Figure S15. TEM images of (a) PM6:L8-BO (107±17 nm), (b) PM6:L8-BO (377±23 nm), (c) PM6:SD62:L8-BO (109±12 nm) and (d) PM6:SD62:L8-BO (395±17 nm), respectively.

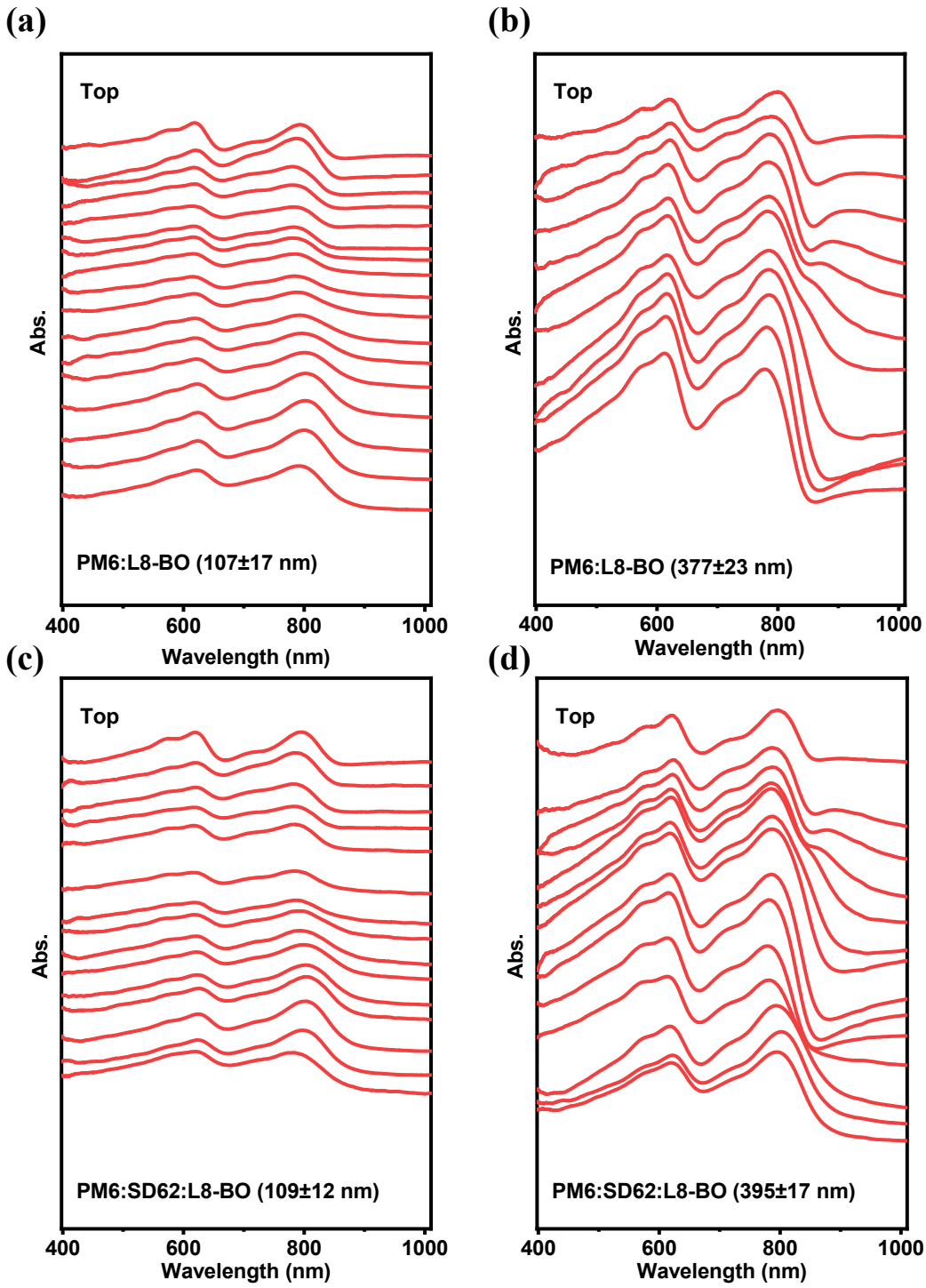

Figure S16. FLAS spectra of (a) PM6:L8-BO (107±17 nm), (b) PM6:L8-BO (377±23 nm), (c) PM6:SD62:L8-BO (109±12 nm) and (d) PM6:SD62:L8-BO (395±17 nm), respectively..

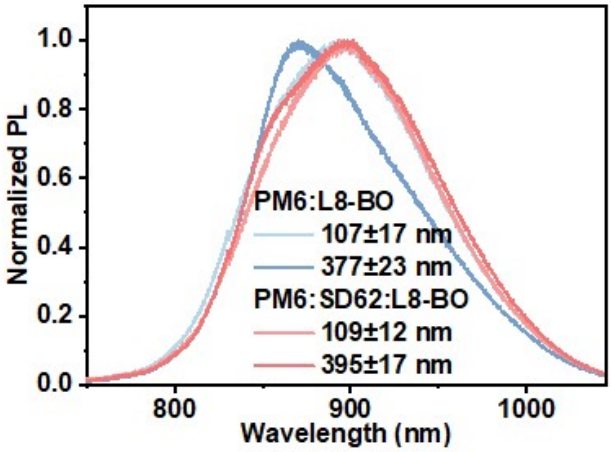

Figure S17. Normalized PL spectra of the binary and ternary OSCs films with different thicknesses excited at 532 nm.

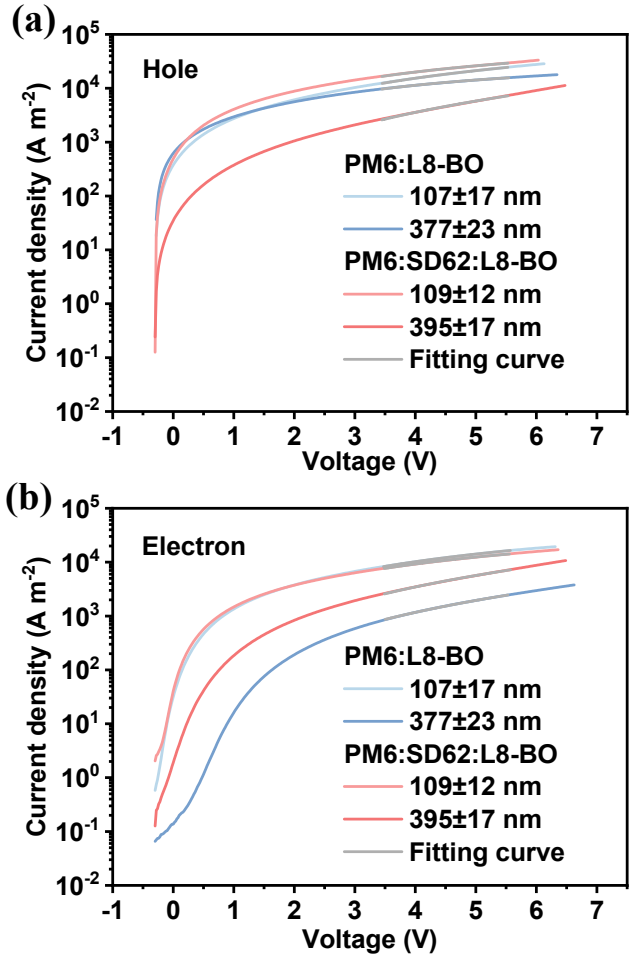

Figure S18. The dark *J-V* characteristics of (a) hole-only devices and (b) electron-only devices for the binary and ternary devices with different thicknesses. The solid lines represented the best fitting using the SCLC model.

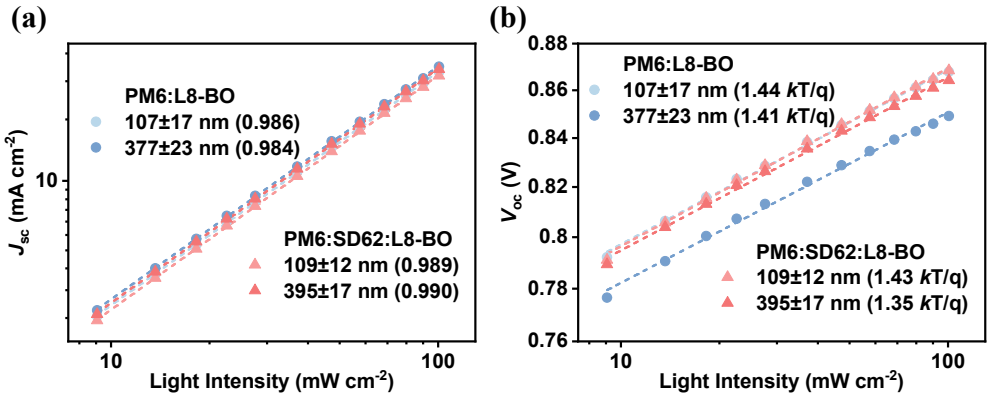

Figure S19. (a) Dependence of short-circuit current density (J_{SC}) on the light intensity of the devices. The dashed lines represent linear fits of the data; (b) Dependence of open-circuit voltage (V_{OC}) on the light intensity of the devices. The dashed lines represent linear fits of the data. The dependence of J_{SC} on light intensity was used to characterize the bimolecular recombination, which could be expressed as $J_{SC} = \beta(I)^{\alpha}$ (α was the exponential factor and β was a constant).[3, 4] The bimolecular recombination was considered less if the value of α was closer to 1. The calculated values of α were 0.986 (for 107±17 nm) and 0.984 (for 377±23 nm) for the binary devices, 0.989 (for 109±12 nm) and 0.990 (for 395±17nm) for the ternary devices. All these values were close to 1, which meant that there was a small amount of bimolecular recombination in both the binary and the ternary systems. And the α values of the ternary devices were closer to 1, suggesting the incorporating of appropriate SD62 could benefit to suppressing the bimolecular recombination. In addition, a stronger dependence of V_{OC} on ln(P_{light}) with the slope (S) > kT/q (k,T and q represented the Boltzmann constant, Kelvin temperature and elementary charge, respectively) was considered to suffer more serious trap-assisted recombination. If the trap-assisted recombination was significant, the slope would be close to 2 kT/q.[5, 6] In this case, the slope values were calculated as 1.44 kT/q (for 107±17 nm) and 1.41 kT/q (for 377±23 nm) for the binary devices, 1.43 kT/q (for 109±12 nm) and 1.35 kT/q (for 395±17 nm) for the ternary devices. It seemed that thick-film devices showed slightly weaker trap-assisted recombination than thin-film devices, which may benefit from the increasing number of carriers along with the increasing thickness of the active layer, so that the proportion of traps in the active layer was smaller. Besides, the binary devices suffered from severer trap-assisted recombination compared with the ternary devices, which indicated that the addition of SD62 could suppress trap-assisted recombination in polymer solar cells.

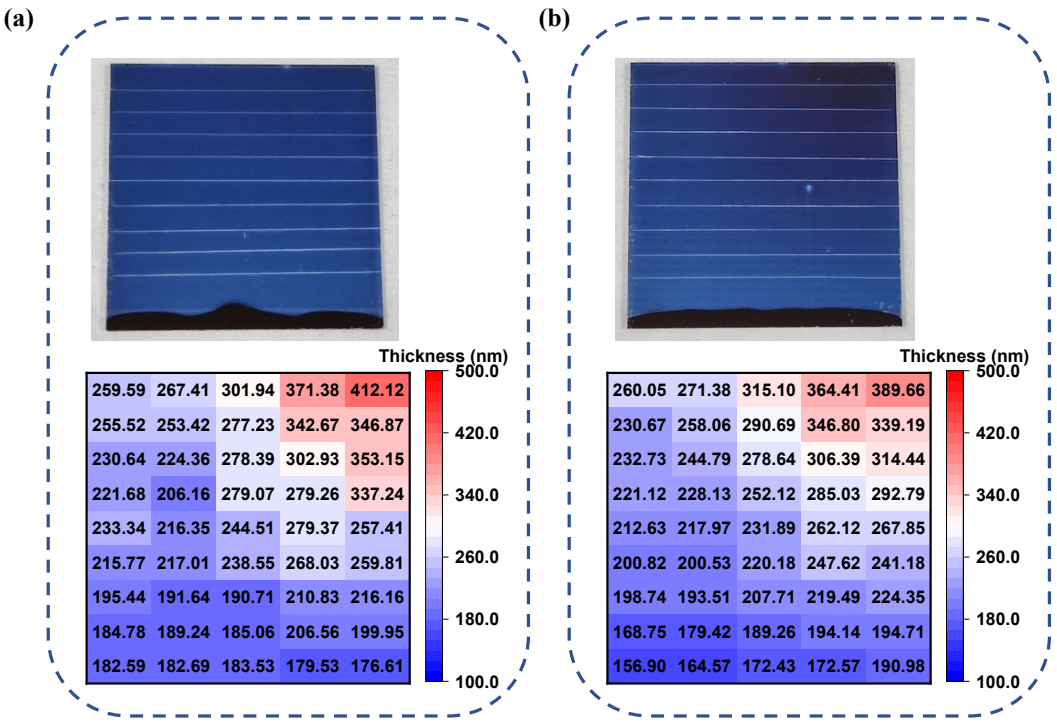

Figure S20. The film thickness distribution of the (a) PM6:L8-BO binary and (b) PM6:SD62:L8-BO ternary systems, respectively.

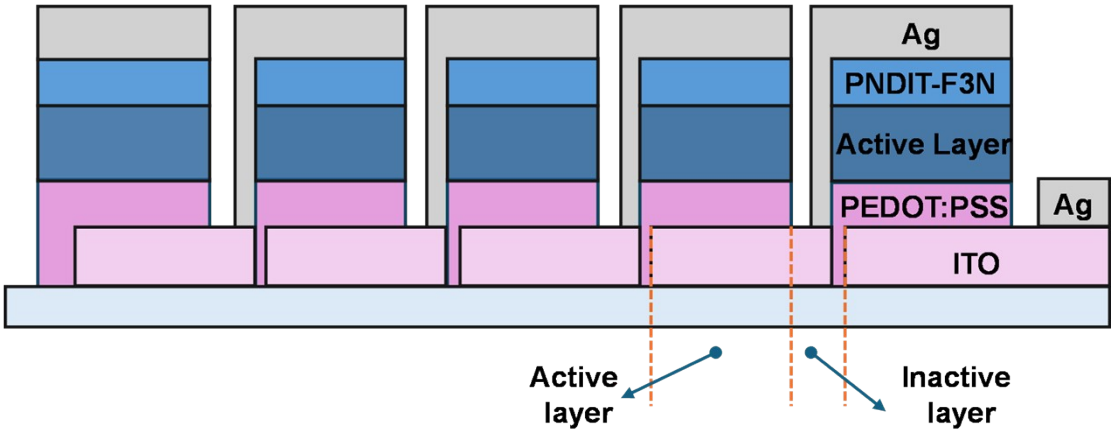

Figure S21. The schematics of the large-area module consisting of five sub-cells monolithically connected in series by ITO-to-Ag interconnects.

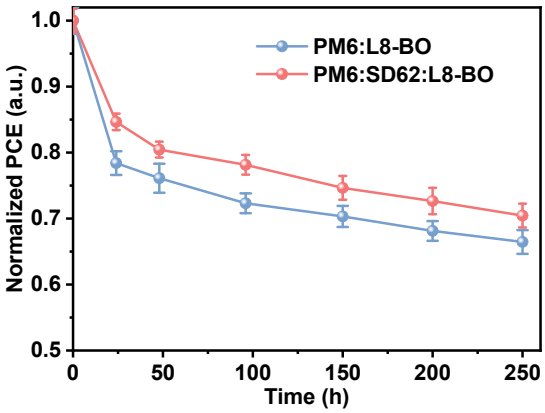

Figure S22. The normalized PCE degradation trends of the large-area modules for the binary and ternary systems, illuminated under one sun.

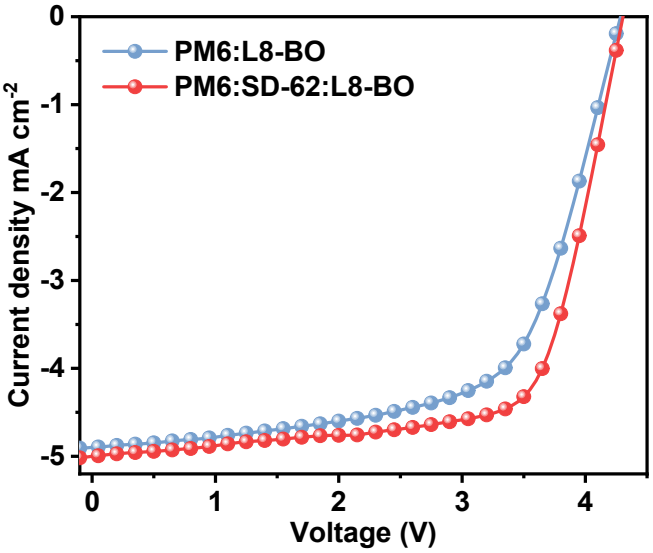

Figure S23. *J-V* characteristics of the binary and the ternary large-area modules fabricated with green solvent (toluene).

Table S4. Photovoltaic parameters of the binary and the ternary large-area modules fabricated with green solvent (toluene).

Active layer	V_{OC} [V]	J_{SC} [mA cm^{-2}]	FF [%]	PCE [%]
PM6: L8-BO[a]	4.29 (4.280±0.08)	4.90 (4.82±0.30)	63.72 (63.01±0.30)	13.38 (13.05±0.15)
PM6:SD62:L8-BO[a]	4.31 (4.30±0.01)	5.00 (4.88±0.20)	70.27 (70.00±0.25)	15.13 (15.00±0.10)

a) The parameters of large-area modules with an effective area of 15.4 cm^2.

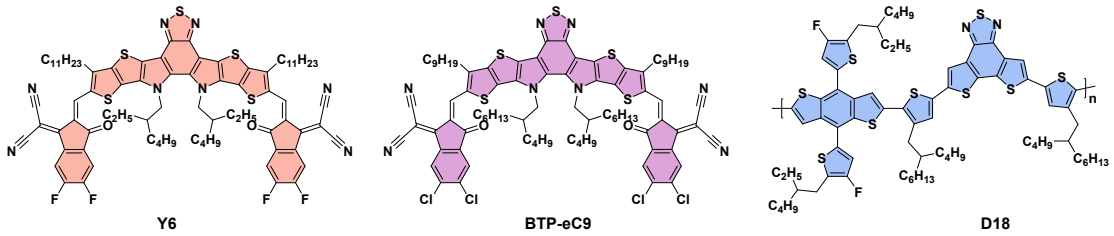

Figure S24. Molecular structures of the investigated organic photovoltaic materials.

References

1 T. Duan, Q. Chen, Q. Yang, D. Hu, G. Cai, X. Lu, J. Lv, H. Song, C. Zhong, F. Liu, D. Yu and S. Lu, *J. Mater. Chem. A*, 2022, **10**, 3009-3017.

2 W. Gao, M. Jiang, Z. Wu, B. Fan, W. Jiang, N. Cai, H. Xie, F. R. Lin, J. Luo, Q. An, H. Y. Woo and A. K. Jen, *Angew. Chem. Int. Ed.*, 2022, **61**, e202205168.

3 R. Sun, T. Wang, Q. Fan, M. Wu, X. Yang, X. Wu, Y. Yu, X. Xia, F. Cui, J. Wan, X. Lu, X. Hao, A. K. Y. Jen, E. Spiecker and J. Min, *Joule*, 2023, **7**, 221-237.

4 Y. Gao, X. Yang, R. Sun, L.-Y. Xu, Z. Chen, M. Zhang, H. Zhu and J. Min, *Joule*, 2023, DOI: 10.1016/j.joule.2023.10.006.

5 J. Guo, Y. Wu, R. Sun, W. Wang, J. Li, E. Zhou, J. Guo, T. Wang, Q. Wu, Z. Luo, W. Gao, Y. Pan, C. Yang and J. Min, *Sol. RRL*, 2021, **5**, 2000704.

6 R. Sun, W. Wang, H. Yu, Z. Chen, X. Xia, H. Shen, J. Guo, M. Shi, Y. Zheng, Y. Wu, W. Yang, T. Wang, Q. Wu, Y. Yang, X. Lu, J. Xia, C. J. Brabec, H. Yan, Y. Li and J. Min, *Joule*, 2021, **5**, 1548-1565.